# Effect of Spin Finish on Fiber/Binder Adhesion in Chemically Bonded Nonwovens

**Sylvie Fourdrin,[1] Maryline Rochery,[1] Léon Gengembre,[2] Pascal Rumeau,[3] Maryline Lewandowski,[1] Manuela Ferreira,[1] Serge Bourbigot[4]**

[1]*Laboratoire de Génie et Matériaux Textiles, UPRES EA2461, Ecole Nationale Supérieure des Arts et Industries Textiles, 9 Rue de l'Ermitage, B.P. 30329, Roubaix Cedex 01 59056, France*
[2]*Laboratoire de Catalyse, UMR CNRS 8010, Université des Sciences et Technologies de Lille, Bat. C3, Villeneuve d'Ascq Cedex 59655, France*
[3]*Institut Français Textile, Habillement, 2 Rue de la Recherche, Villeneuve d'Ascq Cedex 59650, France*
[4]*Laboratoire des Procédés d'Elaboration de Revêtements Fonctionnels, UPRES EA1040, Ecole Nationale Supérieure de Chimie de Lille, B.P. 108, Villeneuve d'Ascq Cedex 59652, France*

Received 3 May 2005; accepted 9 January 2006
DOI 10.1002/app.24098
Published online in Wiley InterScience (www.interscience.wiley.com).

**ABSTRACT:** The purpose of this study is to better understand the mechanisms governing the phenomena of fiber/matrix adhesion by controlling the fiber surface properties. This adhesion is evaluated by studying the micromechanical and thermodynamical behavior of the fiber/matrix interface. The complexity of the interactions at the interface requires a global approach that takes into account the chemistry, morphology, and mechanics. The thermodynamical affinity between the binder and fibers is evaluated by the wetting behavior, whereas the mechanical resistance of the fiber/matrix interface is characterized with the pull-out test. Three distinct approaches are used to classify the different systems according to the nature of the binder and the fiber surface. It is found that there is better adhesion when the spin finish is removed from the fibers, revealing the surface roughness on which the latex can mechanically anchor. © 2006 Wiley Periodicals, Inc. J Appl Polym Sci 102: 4092–4100, 2006

**Key words:** fiber; latex; adhesion; X-ray photoelectron spectroscopy; pull-out

## INTRODUCTION

Chemically bonded nonwovens (NWs) are textile structures obtained from a sheet of directionally or randomly oriented fibers bonded together by an adhesive binder. The most current binders are waterborne latexes, and acrylic latexes represent the predominant class of binders that are used. To attain a better understanding of the mechanisms involved in the adhesion between the fiber and binder, a model acrylic latex formulation has been developed in our laboratory and is compared to a commercial latex. Concerning the choice of the fiber, polyester [poly(ethylene terephthalate) (PET)] fibers were selected because of their widespread use in the NW industry. However, they have an intrinsic poor affinity for the binders, which is in contradiction with the fact that a good uphold of the fiber/matrix composite depends on the adhesion between these two elements.[1–6] The aim of this article is to study the fiber/binder adhesion to determine the different physicochemical parameters that can improve this adhesion, the surface properties in particular. Improving this adhesion will lead to a reduction in binder content for a NW product with the same resistance and a softer feel. The outcome of this work therefore represents economic interest as well as favorable environmental impact because of the binder waste limitations.

In this study, the fibers were unsized (i.e., washed to eliminate spin finish) in order to characterize the ''naked'' fiber and to evaluate the role of the finishing oils on the fiber/binder adhesion. We investigated the physicochemical transformations of the fiber surface by wetting and X-ray photoelectron spectroscopy (XPS) measurements, and atomic force microscopy (AFM) analyses helped us to understand the morphological changes on the fiber surface. The performance of composite materials is largely determined by the fiber/matrix interface properties, which can be measured by one of the most current methods used to evaluate fiber/matrix adhesion: the pull-out test.[7,8] Its principle consists in measuring the force required to extract a fiber from its matrix for different embedded fiber lengths. With these two parameters, it is possible to compute the shear stress or the fracture energy of the interface using different approaches. Among these approaches, three distinct ones were used in this work to classify the different fiber/matrix systems and to study the influence of the surface quality of the fiber on

*Correspondence to:* M. Rochery (maryline.rochery@ensait.fr).
Contract grant sponsors: PRTH, French Nord-Pas de Calais Region.

**TABLE I**
**Characteristics of PET Fibers**

| Young's modulus (GPa) | Tensile strength (MPa) | Elongation (%) | Diameter (μm) | $T_g$[a] (°C) | $T_f$[a] (°C) | Crystallinity[a] (%) |
|---|---|---|---|---|---|---|
| 5.7 ± 0.6 | 396 ± 34 | 63 ± 6 | 38.0 ± 1.4 | 79.8 ± 0.6 | 239 ± 1 | 48 ± 2 |

[a] The results are from DSC analysis.

adhesion. One is based on a stress criterion (Greszczuk's model[9]) and the other two are based on an energy criterion (Gent and Liu's[10] and Yue and Cheung's[11] models).

## EXPERIMENTAL

### Materials

The PET fibers used in the study were from Wellman International; they have a mean count (linear density) of 15.7 dtex and a circular cross section (3-μm diameter, calculated from the fiber count). During the production of polymeric fibers, aqueous solutions of spin finishes are applied to the fiber surface to control the friction and to prevent antistatic problems arising from the high-speed spinning process. These fibers are designated as sized fibers. To facilitate their handling during testing and during the fabrication of the fiber/matrix composite, they were provided in the form of straight continuous filaments. Their main characteristics are provided in Table I. The fibers have to be thermoset before testing, an operation that is necessary for dimensional stability and that is carried out by heating all the sized fibers at 150°C for 20 min.

Two anionic latexes were used in this study. The first one was the commercial acrylic binder Appretan N 9410 (Clariant S.A.), which is composed of acrylic ester and vinyl acetate copolymers. The second latex, a model acrylic binder based on methyl methacrylate and butyl acrylate, was synthesized via a semicontinuous reaction scheme. The preparation of the model latex was carried out in order to obtain latex characteristics similar to those of the commercial binder (Table II). The detailed synthesis procedure that follows a semicontinuous scheme can be found in a previously published article.[12] Both binders are self-crosslinkable at around 150°C.

### Unsizing of fibers

The procedure for fiber unsizing is not clearly defined in the literature because it depends on the formulation of the spin finish. The method used here was developed in our laboratory and is well adapted to the majority of classical spin finishes.[3] For this washing operation the fibers were treated at 30°C in a receptacle placed in an ultrasonic bath, and they underwent six 15-min washing cycles: the first two cycles were done in an apolar solvent and the third one in methanol. In the last three cycles the fibers were washed with deionized water to eliminate the soluble species. Between each cycle the fibers were dried at 40°C for 24 h. Unsized fibers were finally obtained.

### Characterization

#### Wetting

The wetting behavior was studied with PET fibers by dynamic analysis using the tensiometric method. A single filament was suspended from an electronic microbalance (Cahn 322) and weight changes were recorded during the fiber immersion–emersion cycle into the test liquid at a speed of 20 μm/s. Advancing ($\theta_a$) contact angles were calculated using the Wilhelmy equation,[13] neglecting the buoyancy forces from the weight changes ($W$), which were detected during the immersion of the fibers into the test liquid by

$$\cos\theta_a = \frac{W}{p\gamma_L} = \frac{mg}{p\gamma_L} \quad (1)$$

where $g$ is the acceleration due to gravity, $p$ is the fiber perimeter, and $\gamma_L$ is the surface tension of the liquid determined by a Wilhelmy balance technique with a platinum plate.

**TABLE II**
**Characteristics of Chemical Binders**

| Latex | Surface tension (mN/m) | pH | Particle size (nm) | Dry content (%) | $T_g$[a] (°C) | Young's modulus[a] (MPa) |
|---|---|---|---|---|---|---|
| Commercial | 31.1 ± 0.7 | 5.5 | 200 | 45 | −13.2 ± 0.4 | 0.76 ± 0.04 |
| Model | 36.7 ± 0.5 | 8.4 | 209 | 41 | −12.6 ± 0.2 | 1.19 ± 0.12 |

[a] The results are from differential scanning calorimetry ($T_g$) and tensile (Young's modulus) analyses on crosslinked latex films that were coalesced at room temperature for approximately 2 days and cured at 160°C for 20 min for the commercial binder and 45 min for the model one.

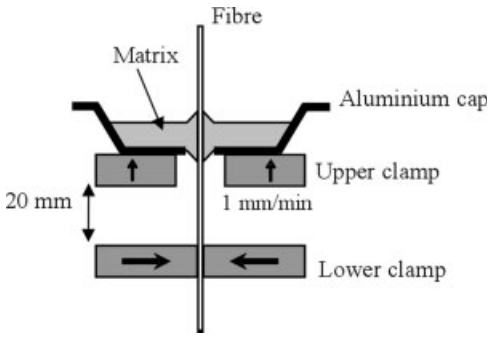


**Figure 1** A schematic representation of the pull-out test.

XPS

The chemical composition of the fiber surface was investigated by means of XPS on sized and unsized fibers. The analyses were performed on a Leybold LHS10 spectrometer. The photoemission was excited by Mg Kα radiation ($h\nu = 1253.6$ eV) at an anode voltage of 13 kV and an anode current of 24 mA. The analyzer was working in a 50-eV constant pass energy mode. The pressure in the analysis chamber was $10^{-6}$–$10^{-7}$ Pa when the polymer sample underwent X-ray exposure. To overcome charging effects, all peak binding energies were referenced to the C1s binding energy of the hydrocarbon component, which was set at 284.7 eV. The C1s spectra were acquired by means of a data acquisition system. Before fitting, the peaks were smoothed by a least-squares method and the background was linearly subtracted. The peaks were fitted by a procedure based on the independent variations of parameters such as the peak positions, widths, and heights and Gaussian–Lorentzian peak shape mixed ratios.

Pull-out test

In this study a cylindrical drop geometry was developed.[14,15] The composite was set up as follows: a small hole (diameter = 100 μm) was made in the middle of a DSC aluminum cap. A fiber was introduced into this hole and held vertically. A small quantity of latex was

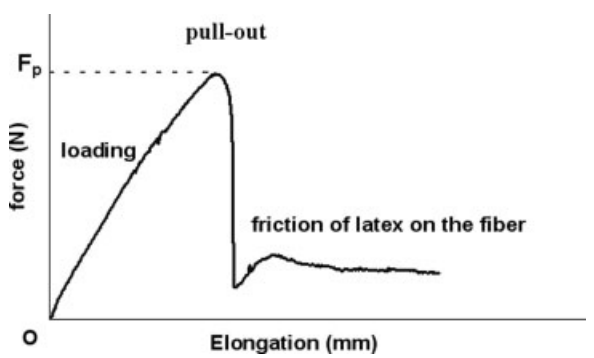


**Figure 2** The typical force–elongation curve obtained during a pull-out test.

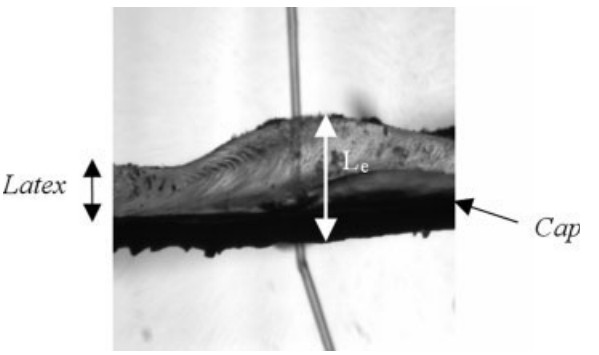


**Figure 3** The determination of the embedded length ($L_e$) by optical microscopy.

then put in the cap using a syringe. The preparation then underwent a thermal treatment of 8 h at 40°C, followed by 20 min for the commercial latex (45 min for the model latex) at 160°C to crosslink the binder. The pull-out test was done on a Zwick tensile apparatus. The cap was put on the upper clamp, and the free end of the fiber was set up in the lower clamp. The distance between clamps was 20 mm. The crosshead speed was set to 1 mm/min (Fig. 1). The force applied on the fiber was then recorded against the elongation. Figure 2 presents a typical example of a force/elongation curve and exhibits several zones: loading, pull-out, and friction. For each test, the pull-out force necessary to loosen the fiber from the matrix was recorded and the length of fiber embedded in the matrix was determined with an optical microscope after the pull-out test (Fig. 3).

## RESULTS AND DISCUSSION

### Characterization of fibers

Wettability of fibers

The contact angle between the fibers and water ($\gamma_L = 72.6$ mN/m) was determined on sized and unsized fibers. In order to study the influence of several successive wettings, two wetting cycles were carried out. This enabled the highlighting of the exchanges of matter or the various interactions between fiber and liquid. Table III shows the evolution of the wettability of PET fibers (average and standard deviations on seven fiber samples) according to the wetting cycle and the nature of the fibers.

The contact angle between the water and unsized PET fiber is 81°. This value was obtained during the

**TABLE III**
**Evolution of Contact Angle of Sized and Unsized Fibers in Water**

| | First cycle | Second cycle |
|---|---|---|
| Sized fiber | 71.0 ± 1.5 | 78.0 ± 2.5 |
| Unsized fiber | 81.0 ± 0.7 | 81.0 ± 0.5 |

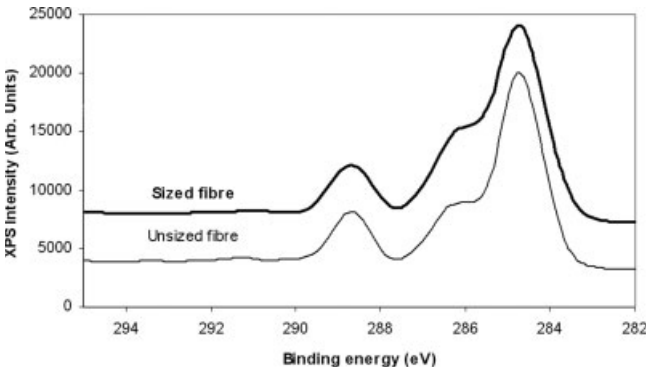


**Figure 4** The evolution of the C1s core-level spectra of PET fibers.

two wetting cycles and is close to the theoretical value[16] (82°); thus, we can assume that the surface of the unsized fiber is clean. Concerning the sized fiber, its contact angle with water was 71° during the first cycle, a lower value than the one obtained with the unsized fibers (81°). The spin finish thus improved the wettability of the fibers with water. During the second cycle, the contact angle obtained was higher (78 vs. 71°). We propose two assumptions to explain this phenomenon: either the surfactants present in the spin finish reorganize on the surface of the fiber in contact with water or a part of the components of the spin finish (particularly the surfactants) migrate into the water. However, the measurement of the surface energy of the water after the tests did not reveal any modification. If there was migration of surfactant, it was negligible. We also noticed that the dispersion of the results was larger with a sized fiber than with an unsized one. We can attribute this phenomenon to the variations from one fiber to another of the contact angles following the reorganization or migration kinetics of the spin finish in contact with the water.

## Chemical surface analysis of fibers

The chemical composition of the fiber surfaces was investigated using XPS analyses. Figure 4 shows the

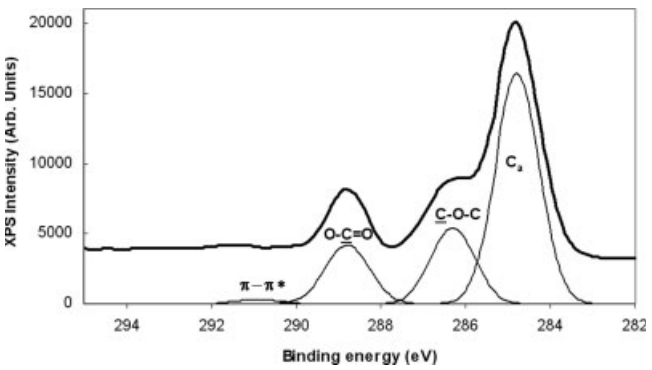


**Figure 5** The C1s spectrum deconvolution of unsized PET fibers.

**TABLE IV**
**Relative Component Intensities (% Total Peak Areas) of Deconvoluted C1s Core-Level Spectra of PET Fibers**

| | $C_a$ | C—O—C | O—C=O | π–π* |
|---|---|---|---|---|
| Sized fibers | 60.8 | 25.3 | 12.9 | 1 |
| Unsized fibers | 64.9 | 19.5 | 14.1 | 1.5 |
| Theoretical[a] | 60 | 20 | 20 | — |

[a] Deduced from the repeat unit (cf. Fig. 6).

C1s core-level spectra of sized and unsized PET fibers. The best fit for decomposition of the C1S spectra was obtained when using a full width at half-maximum of 1.7 eV for each peak component. A typical example of deconvoluted spectra of XPS core-level C1S spectra of unsized PET fibers is given in Figure 5. The C1S spectra of sized and unsized fibers present a high-intensity peak at 284.7 eV, which characterizes the carbon atoms not bonded to oxygen atoms and identified as aromatic and/or aliphatic carbons ($C_a$). The shoulder appearing at 286.3 eV on the high binding energy side of the peak is due to carbon in the group C—O—C, whereas the peak at 288.7 eV corresponds to the carbon atoms positively polarized by neighboring oxygen atoms (O—C=O). A small shake-up structure attributable to the aromatic ring $\pi \rightarrow \pi^*$ transition is also detected in the high binding energy region (291 eV). All the results for binding energies are in good agreement with the literature data.[17–20]

The experimental relative areas under C1S envelopes are presented in Table IV and compared to the theoretical data deduced from the repeat unit of PET in Figure 6. The elementary compositions of oxygen relative to carbon determined from the O1s and C1s signals (O/C atomic ratios) are listed in Table V. The $C_{ox}/C_a$ ratios are also reported: this ratio is defined in eq. (2) and corresponds to the ratio of carbon atoms bonded and not bonded to oxygen atoms, respectively:

$$\frac{C_{ox}}{C_a} = \frac{C—O—C + O—C=O}{C_a} \qquad (2)$$

The obtained C1S values are not similar to the expected theoretical values for the stoichiometric PET. The same observation is made for the O/C atomic ratios. These results are not surprising for the sized fibers but are more unexpected for the unsized ones. This can be explained by the presence of a layer of contamination on the unsized fiber surface. Indeed, any surface, even if it is not very reactive, can recover different species

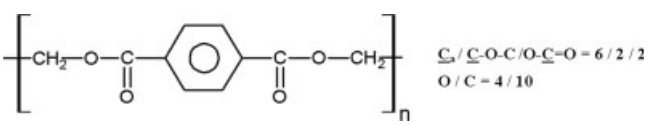


**Figure 6** The repeat unit of PET.

**TABLE V**
**Elementary Composition of Oxygen Relative to Carbon (O1s/C1s) and $C_{ox}/C_a$ Ratios for Sized and Unsized PET Fibers**

| PET fiber | O1s/C1s | $C_{ox}/C_a$ |
|---|---|---|
| Sized | 0.39 | 0.63 |
| Unsized | 0.34 | 0.52 |

that are deposited or adsorbed during the handling or treatments of the sample.

The sized and unsized fibers show different O/C atomic ratios (0.39 and 0.34, respectively) and C1S component concentrations. The *C*—O—C contribution to the total C1S peak was higher for the sized fibers (25.3%) than for the unsized ones (19.5%). This suggests that the sized surface contained more ether groups htat probably come from the spin finish.

The $C_{ox}/C_a$ ratio jumps from 0.52 for the unsized fibers to 0.63 for the sized ones, indicating a higher level of oxygen-based functional groups at the surface. The higher O/C atomic ratio for the sized fibers confirms this assumption. The oxidation of the fiber surface is thus more important for the sized fiber than for the unsized fiber. These results explain the better wettability of sized fibers that was observed.

## Characterization of fiber/matrix interface

### Thermodynamical affinity between binder and fibers

The thermodynamical compatibility between the different PET fibers and binders is evaluated by the wetting behavior. A weak contact angle implies strong thermodynamical adhesion whereas a bad affinity between fiber and matrix is characterized by an important contact angle.

Measurements were performed at room temperature on sized and unsized fibers. The results obtained as an average of seven tests are gathered in Table VI.

We first note that the contact angles on sized fibers are lower than those obtained on unsized ones. Sizing thus improved the wetting of the fibers for both latexes: by 33% for the model latex and 54% for the commercial one. This result can be explained by the polarity of the surface of sized fibers being more significant than that of unsized fibers (see XPS results), thus improving the wettability with the two latexes. The commercial latex gives slightly lower contact angles than the model one. This is probably due to a better choice of surfactants in the commercial formulation. Indeed, the commercial latexes generally contain several surfactants of different natures, leading to better chemical compatibility with sizing, whereas our model latex contained only one surface-active anion.

**TABLE VI**
**Fiber/Latex Contact Angle**

| Latex | Commercial | Model |
|---|---|---|
| Sized fiber | 23 ± 4 | 44 ± 2 |
| Unsized fiber | 50 ± 3 | 66 ± 2 |

### Single fiber pull-out test

Before presenting the experimental results, it is necessary to recall first the theory used in the pull-out test, namely, the models of Greszczuk,[9] Gent and Liu,[10] and Yue and Cheung.[11] Greszczuk's analysis[9] considers that the interphase around the embedded fiber undergoes a shearing deformation during the pull-out test and supposes elastic behavior of the matrix. This implies that there is a shear gradient along the interface, and this test gives a value of the average shear stress ($\tau_a$) defined by

$$\tau_a = \frac{F_p}{2\pi r L_e} \tag{3}$$

where $F_p$ is the pull-out force, $r$ is the fiber radius, and $L_e$ is the embedded length.

However, the $\tau_a$ is not rigorously representative of adhesion because it depends on the embedded length. The shear stress is maximum at the point of emergence and solicitation of the fiber, and it is equal to zero at the other end. Under these conditions for a given composite system, the most representative value for the adhesion is the maximum value of the interfacial shear stress ($\tau_{max}$) according to

$$\tau_a = \tau_{\max} \frac{\tanh(\alpha L_e)}{\alpha L_e} \tag{4}$$

in which $\alpha = \sqrt{2G_i/b_i r E_f}$, where $b_i$ represents the thickness of the interface, $G_i$ is the interface shear modulus, and $E_f$ is the Young's modulus of the fiber.

The $\tau_{max}$ cannot be directly determined from experiments because it corresponds to an embedded length of zero. In practice, $\tau_{max}$ is determined as follows: pull-out tests are carried out on a series of fiber/matrix composites with different embedded fiber lengths. The

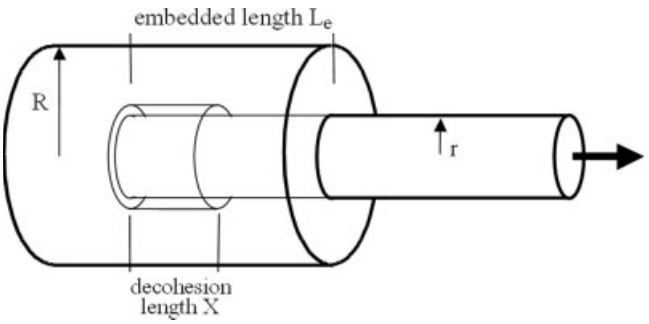


**Figure 7** The pull-out of a rigid fiber in an elastic matrix showing the decohesion zone of length *X*.

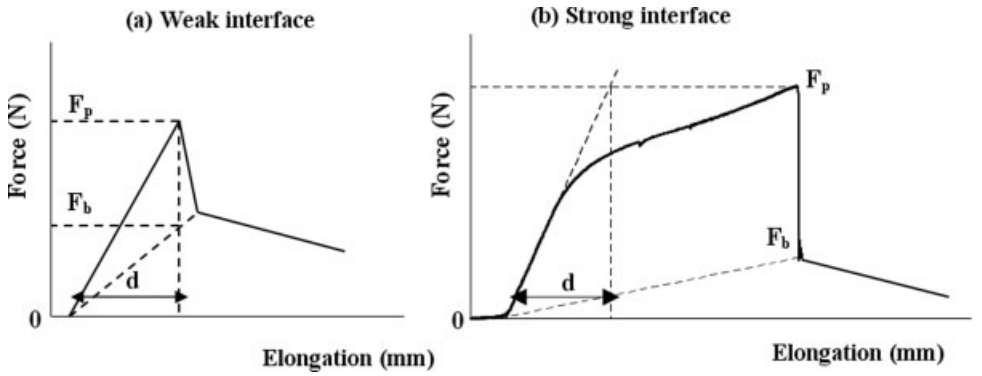


**Figure 8** A graphical determination of displacement ($d$) for a pull-out test (a) with a weak fiber/matrix interface according to Yue and Cheung[11] and (b) with a strong fiber/matrix interface according to our analysis.

experimental points are plotted on a graph of $\tau_a$ versus $L_e$ [eq. (3)]. The theoretical curve of Greszczuk[9] [eq. (4)] is then plotted on the same graph: the values of $\alpha$ and $\tau_{max}$ in Greszczuk's equation are adjusted to attain the best fit using a least-squares curve-fitting program.

The model of Gent and Liu is based on a simple linear analysis of the fracture.[10] For a relatively rigid fiber embedded in a soft matrix, a simple energy balance between work done by the applied force, energy expended in debonding, and elastic energy stored in the newly debonded material leads to eq. (5):

$$F_p^2 = 4\pi A r E_m G_i \tag{5}$$

where $G_i$ is the energy of interfacial fracture; $E_m$ is the Young's modulus for the polymeric matrix, assumed to be linearly elastic; and $A$ is the cross-sectional area of the sample in which the deformation energy is really stored (cylindrical section of radius $R$, see Fig. 7). This relation does not conceptually translate the dependence of $F_p$ according to the $L_e$. It can be applied only for $L_e = 0$.

According to Gent and Liu,[10] the contribution of friction between the fiber and the matrix is especially large when $L_e > R$. They consider the increment in pull-out force, ($\partial F$) due to frictions

$$\partial F = 2\pi r \mu p \partial X \tag{6}$$

where $\mu$ is the friction coefficient, $p$ is the compressive stress, and $X$ is the debonded length (Fig. 7).

If the compressive stress is set up by the frustrated Poissonian contraction of an incompressible elastic matrix material in the form of a thin tube surrounding the fiber, then $p$ is given by

$$P = \frac{F_p}{3\pi R^2} \tag{7}$$

where $F_p$ is the total pull-out force including friction.

After integration, the relation between $F_p$ and X is

$$F_p = F_0 \exp\left(\frac{2\mu r X}{3R^2}\right) \tag{8}$$

where $F_0$ is the pull-out force for $X = 0$. This result is based on the assumption that $\mu$ is constant. When there is total pull-out, the model has to be adapted by replac-

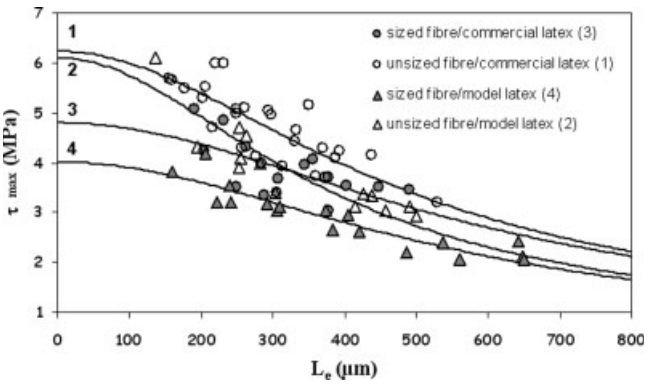


**Figure 9** The shear stress ($\tau_a$) versus the embedded length ($L_e$) according to Greszczuk's[9] model for different PET fiber/latex systems.

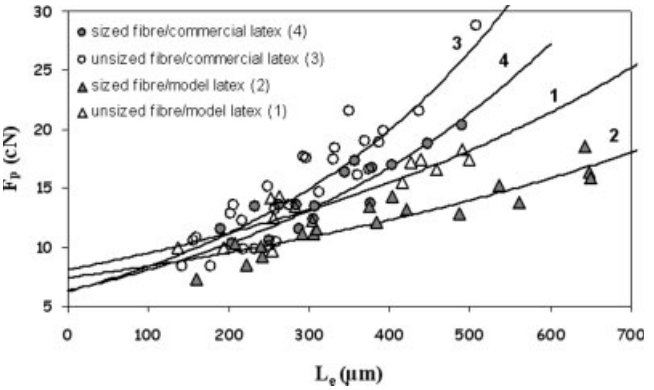


**Figure 10** The pull-out force ($F_p$) versus the embedded length ($L_e$) according to the model of Gent and Liu[10] for different PET fiber/latex systems.

**TABLE VII**
**Pull-Out Test Results of Fiber/Latex Composites**

| | | Greszczuk model | | | Gent and Liu model | | | | | |
|---|---|---|---|---|---|---|---|---|---|---|
| Latex | Fiber | $\tau_{max}$ (MPa) | $r^2$ | Conf. limit (MPa) | $G_i$ (kJ/m$^2$) | $r^2$ | Conf. limit (kJ/m$^2$) | μ | $r^2$ | Conf. limit |
| Commercial | Sized | 4.8 | 0.64 | 3.9–5.6 | 2 | 0.83 | 1.2–3.1 | 0.47 | 0.83 | 0.35–0.59 |
| | Unsized | 6.2 | 0.74 | 5.6–6.8 | 2 | 0.84 | 1.4–2.8 | 0.57 | 0.84 | 0.48–0.66 |
| Model | Sized | 4 | 0.85 | 3.6–4.4 | 1.4 | 0.84 | 1.1–1.9 | 0.25 | 0.84 | 0.20–0.31 |
| | Unsized | 6.1 | 0.83 | 5.1–7.1 | 1.7 | 0.83 | 1.2–2.4 | 0.32 | 0.83 | 0.23–0.41 |

The results were determined using Greszczuk's model[9] ($\tau_{max}$) and Gent and Liu's model[10] ($G_i$ and μ) with their correlation coefficients ($r^2$) and confidence limits at 95%.

ing $X$ with the $L_e$ to obtain a relation between the pull-out force and $L_e$. The values for $F_0$ and μ are then determined as follows: pull-out tests are carried out on a series of fiber/matrix composites with different embedded fiber lengths. The experimental points are plotted on a graph of $F_p$ versus $L_e$. The theoretical curve of Gent and Liu[10] [eq. (8)] is then plotted on the same graph: the value of $F_0$ and μ in Gent's equation are adjusted to attain the best fit. We can then calculate $G_i$ from eq. (5) considering that $R = 50$ μm, which is the radius of the hole in the cap. We assume that only this corresponding cylinder of the matrix undergoes deformation.

Yue and Cheung[11] propose an original graphic approach of the problem, which uses the residual force after pull-out ($F_b$) as well as the elongation of the fiber [Fig. 8(a)]. They define $d$ as the displacement when $F = F_p$. The $G_i$ value is given by

$$G_i = \frac{0.5(F_p - F_b)d}{2\pi r L_e} \quad (9)$$

In the case of a strong interface between the fiber and matrix and more particularly for high embedded lengths, complete debonding occurs in the plastic deformation zone of the fiber, and $d$ as well as $G_i$ are overestimated. In this case, the $d$ value is obtained by extrapolation and by considering purely elastic behavior of the fiber as shown in Figure 8(b). The $G_i$ data obtained represent the average for about 20 pull-out tests for different embedded lengths.

The experimental points and theoretical curves of Greszczuk[9] and Gent and Liu[10] are plotted in Figures 9 and 10, respectively, and the results are tabulated in Table VII.

From the experimental force/elongation curves (Fig. 2) and eq. (9), the $G_i$ is determined using the model of Yue and Cheung[11] for each fiber/matrix composite. The values of $G_i$ and their standard deviations are represented in Figure 11. Note that the values of $G_i$ calculated from the model of Gent and Liu[10] are higher than those calculated from the model of Yue and Cheung.[11] One of the reasons may be the underestimation of the radius for the matrix that is really undergoing the deformation: only the hole made in the cap is taken into account, which probably resulted in an overestimation of $G_i$.

Concerning the Gent and Liu model,[10] the important standard deviations of $G_i$ do not allow the influence of sizing on the fiber/matrix adhesion to be clearly put into evidence. Nevertheless, this approach has the advantage of giving an estimation of the friction coefficient between the fiber and matrix, which is an essential parameter.

The results from the analyses of Greszczuk[9] and Yue and Cheung[11] reveal better adhesion on unsized fibers than on sized fibers for the two latexes. We can thus put forth two assumptions:

1. either the presence of spin finish on the fiber is unfavorable to the fiber/latex adhesion or
2. the roughness of the unsized fiber surface allows better mechanical anchoring of the binder on the fiber compared to the smoother sized fibers.

However, measurements of the contact angles between the fibers and the two latexes highlighted a better thermodynamical affinity between the sized fibers and the two binders. This result thus enables us to dismiss the first assumption.

AFM images (Fig. 12) reveal that unsizing can lead to a greater roughness of the fiber surface, which can

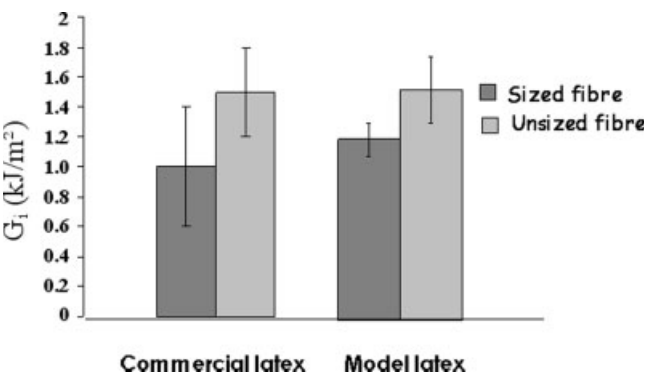


**Figure 11** The interface shear modulus ($G_i$, kJ/m$^2$) values and standard deviations of the fiber/latex composites calculated from pull-out tests using the model of Yue and Cheung.[11]

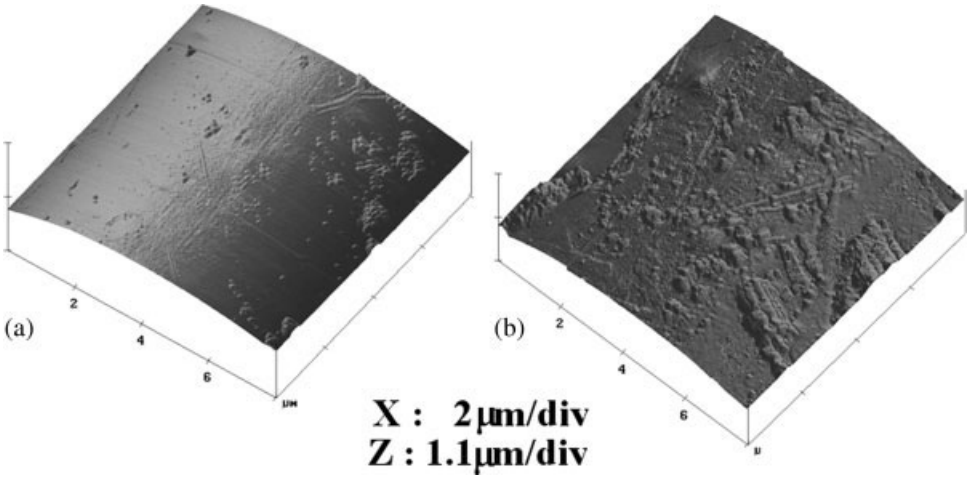


**Figure 12** Three-dimensional views of AFM images of the PET fiber surface: (a) initial sized and (b) unsized.

play a major role in fiber/matrix adhesion: the surface of the sized fiber is found to be relatively smooth compared to the unsized fiber. The film layer of spin finish whose function is to protect the fiber against thermal and/or mechanical solicitations during production and processing has covered the surface irregularities. This is confirmed by the friction coefficients in Table VII, which are higher for the unsized fibers than for the sized ones. The roughness of unsized fibers increases the mechanical anchoring of the binders on the fiber and consequently the adhesive resistance of the fiber/matrix interface. The second assumption seems to be more plausible to explain the better results obtained in adhesion on unsized fibers.

## CONCLUSION

The purpose of this study was to attain better knowledge of the mechanisms governing the phenomenon of adhesion between a fiber and a latex matrix. We saw the nonnegligible role of the spin finish on the surface properties of fibers and on the adhesive resistance of the fiber/matrix interface.

The wetting measurement showed that the fibers presented smaller contact angles with the commercial latex, in agreement with the smaller surface tension of this industrially formulated latex. XPS analysis on sized and unsized fibers demonstrated that the spin finish increased the oxidation of the fiber and, accordingly, its wettability with water and the two latexes (commercial and model). In parallel, AFM analysis of the fiber surface revealed a greater roughness for the unsized fibers compared with the sized ones, as well as a uniform distribution of spin finish on the fiber. Concerning the characterization of the fiber/matrix interface, even if the spin finish contributed to better thermodynamical affinity with the commercial and model latexes, the pull-out test, through the models of Greszczuk[9] and Yue and Cheung,[11] highlighted better adhesion on unsized fibers for the two latexes. From the friction coefficients calculated with the Gent and Liu model,[10] we showed that this might be associated with a higher surface roughness in the case of unsized fibers, facilitating the mechanical anchoring of latex. These results confirmed that the mechanisms that govern adhesion between two materials are very complex and the influencing factors on adhesion are the result of a combination of different mechanisms. However, it is probable that the dominant mechanism is the one that will dictate the quality of the fiber/matrix adhesion. In our case, surface roughness was the prevalent parameter in the adhesion between the acrylic latex and polyester fibers. Thus, thermodynamical affinity was a necessary condition to obtain good adhesion between the two materials, but it was not a sufficient condition.

This work was carried out in the framework of the PRTH Project. lt was performed in collaboration with the Institut Français du Textile et de l'Habillement and supported by the French Nord-Pas de Calais Region. The authors thank Wellman International for providing the PET fibers and Clariant S.A. for supplying the commercial acrylic binder. We are particularly indebted to Dr. Alain Blanc for helpful discussions. Dr. Michel Nardin is also acknowledged for his assistance in the interpretation of the pull-out results with the model of Gent and Liu.[10] Thanks are also due to Mr. François Dassonville from GEMTEX for experimental assistance in the AFM experiments.

### References

1. Epstein, M.; Shishoo, R. J Appl Polym Sci 1993, 50, 863.
2. Lopez-Manchado, M. A.; Arroyo, M. Rubber Chem Technol 2001, 74, 189.
3. Campagne, C. Ph.D. Thesis, Université des Sciences et Technologies de Lille, Lille, France, 2001.
4. Manenq, F.; Carlotti, S.; Mas, A. Angew Makromol Chem 1999, 271, 11.

5. Carlotti, S.; Mas, A. J Appl Polym Sci 1998, 69, 2321.
6. Delfolie, C.; Depecker, C.; Lefebvre, J. M. J Mater Sci 1999, 34, 481.
7. Broutman, L. J. Interfaces in Composites. ASTM STP 452; American Society for Testing and Materials: Philadelphia, PA, 1969; p 27.
8. Miller, B.; Gaur, U.; Hirt, D. E. Compos Sci Technol 1991, 42, 207.
9. Greszczuk, L. B. Interfaces in Composites. ASTM STP 452; American Society for Testing and Materials: Philadelphia, PA, 1969; p 42.
10. Gent, A. N.; Liu, G. L. J Mater Sci 1991, 26, 2467.
11. Yue, C. Y.; Cheung, W. L. J Mater Sci Lett 1991, 10, 1335.
12. Fourdrin, S.; Rochery, M.; Lewandowski, M.; Ferreira, M.; Bourbigot, S. J Appl Polym Sci 2005, 99, 1117.
13. Wilhelmy, L. Ann Phys 1863, 119, 177.
14. Devaux, E.; Caze, C. Compos Sci Technol 1999, 59, 459.
15. Devaux, E.; Caze, C. Compos Sci Technol 1999, 59, 879.
16. Wu, S. Polymer Interfacial Adhesion; Marcel Dekker: New York, 1982.
17. Friedrich, J.; Loeschcke, I.; Frommelt, H.; Reiner, H.-D.; Zimmermann, H.; Lutgen, P. Polym Degrad Stab 1991, 31, 97.
18. Grimblot, J. L'Analyse de Surface des Solides par Spectroscopies Électroniques et Ioniques. Collection Mesures Physiques; Édition Masson: Paris, 1995.
19. Lopez, G. P.; Castner, D. G.; Ratner, B. D. Surf Interface Anal 1991, 17, 267.
20. Castner, D. G.; Ratner, B. D. Surf Interface Anal 1990, 15, 479.